Journal of Photonics for Energy

PhotonicsforEnergy.SPIEDigitalLibrary.org

Impact of optically nonuniform luminescence coupling effect to the limiting cell conversion efficiency in InGaP/GaAs/Ge triple junction solar cell

Bernice Mae F. Yu Jeco
Tomah Sogabe
Ryo Tamaki
Nazmul Ahsan
Yoshitaka Okada

SPIE.

Bernice Mae F. Yu Jeco, Tomah Sogabe, Ryo Tamaki, Nazmul Ahsan, Yoshitaka Okada, "Impact of optically nonuniform luminescence coupling effect to the limiting cell conversion efficiency in InGaP/GaAs/Ge triple junction solar cell," *J. Photon. Energy* **7**(3), 035501 (2017), doi: 10.1117/1.JPE.7.035501.

Impact of optically nonuniform luminescence coupling effect to the limiting cell conversion efficiency in InGaP/GaAs/Ge triple junction solar cell

Bernice Mae F. Yu Jeco,[a,b,*] Tomah Sogabe,[b,c] Ryo Tamaki,[b] Nazmul Ahsan,[a,b] and Yoshitaka Okada[a,b]

[a]The University of Tokyo, Graduate School of Engineering, Department of Advanced Interdisciplinary Studies, Meguro-ku, Tokyo, Japan

[b]The University of Tokyo, Research Center for Advanced Science and Technology, Meguro-ku, Tokyo, Japan

[c]University of Electro-Communications, i-Powered Energy Research Center, Chofu, Tokyo, Japan

Abstract. The impact of nonuniform spatial distribution of the luminescence coupling (LC) effect to the limiting cell conversion efficiency of multijunction solar cells (MJSCs) has been investigated. For this purpose, the laser beam induced current distribution maps of the limiting bottom cell have been acquired experimentally under varying middle-to-bottom cell LC efficiencies. The minimum and the maximum LC efficiencies demonstrated were 8.5% and 69%, respectively. To further analyze the measurement results, a quasi-two-dimensional simulation model considering the spatially nonuniform nature of the LC effect has been developed. A good agreement between the simulation and the measurement results suggests that the nonuniform LC current distribution is induced by optical phenomena such as photon escape and internal reflection. This nonuniformity then causes the absolute conversion efficiency of the limiting cell to be reduced by 1.35% at maximum LC efficiency. This reduction, when suppressed, can yield higher limiting cell conversion efficiency, which in turn may improve the overall MJSC conversion efficiency. [DOI: 10.1117/1.JPE.7.035501]

Keywords: current mapping; current mismatch; luminescent coupling; multijunction solar cell; tandem solar cell.

Paper 17040 received Apr. 12, 2017; accepted for publication Jul. 5, 2017; published online Aug. 4, 2017.

1 Introduction

Multijunction solar cells (MJSCs) are high-efficiency solar cell devices composed of multiple semiconductor materials stacked together to allow photon-to-electron conversion in a wider range of the solar spectrum.[1,2] These devices have demonstrated conversion efficiencies beyond 37% under global air-mass 1.5 spectrum.[3] One way to further improve MJSC conversion efficiency is to optimize the luminescence coupling (LC) effect, which is described as the absorption of photons emitted from a higher bandgap subcell to a lower bandgap subcell.[4–9] Studies on its electrical properties have been extensively conducted using the current–voltage ($J-V$) characterizations and one-dimensional modeling.[10–12] However, to the best of our knowledge, whether or not the spatial distribution of the LC effect has a significant impact on the limiting cell conversion efficiency of a series-constrained MJSC has not been probed yet in detail. Thus, we have investigated the impact of in-plane profile of LC current generation in MJSCs, which has been found to be nonuniformly distributed,[13] to the limiting cell conversion efficiency. For this purpose, we have characterized commercial MJSCs using the laser beam induced current

*Address all correspondence to: Bernice Mae F. Yu Jeco, E-mail: yujeco@mbe.rcast.u-tokyo.ac.jp

(LBIC) mapping method and developed a quasi-two-dimensional (Q-2D) simulation model. Here, the MJSC sample has been modeled in 2-D using an electrical simulation circuit model while the nonuniform optical profile of the LC effect has been modeled in three dimensions. Good agreement of the measurements with the simulation model results suggests that the nonuniformity of the LC effect is optically induced. Moreover, it is less likely caused by edge recombination, which is typically modeled using electrical circuits alone[14–18] (see Appendix A.1). We have found that the absolute conversion efficiency reduction of the limiting cell due to nonuniform LC current generation is 1.35% at maximum LC efficiency. Addressing this reduction can increase the limiting cell conversion efficiency, which in effect may improve the overall MJSC conversion efficiency.

2 Methodology

2.1 *Experimental Setup*

We have characterized commercial triple junction solar cells (3JSCs) whose area is 0.31 cm^2. The top, middle, and bottom cells of the 3JSC are indium gallium phosphide (InGaP), gallium arsenide (GaAs), and germanium (Ge), respectively. The samples were characterized by LBIC mapping method at room temperature, in which the Ge bottom cell was made current limiting.[13] To measure the spatial distribution of the photocurrent generated by direct light source excitation and by the LC effect in the limiting Ge bottom cell, a 1064-nm laser and a 785-nm laser were used, respectively. Both lasers were set to a switching frequency of 3500 Hz and their spot diameters are 100 and 50 μm, respectively. These lasers move in a horizontal and vertical manner, scanning upon the sample stage. In addition, continuous illumination 430- and 660-nm LEDs were used to make the Ge bottom cell current limiting. For the case of 1064-nm laser excitation, we used an attenuation filter (transmission, $T \approx 10\%$) for the laser to ensure that the Ge bottom cell remains current limiting. As an additional reference, we measured the spatial distribution of the adjacent GaAs middle cell by employing continuous 430-, 970-, and 1550-nm LEDs to make it current limiting and a 785-nm laser to directly excite it. For this setup, an attenuation filter ($T \approx 10\%$) was also used to ensure that the GaAs middle cell remains current limiting. The specifications of the continuous LED and pulsating laser sources employed in the setup are summarized in Tables 2 and 3 and Appendix A.2, respectively.

2.2 *Quasi-Two-Dimensional Simulation Model*

To analyze the measurements, we have developed a simulation model that satisfies both the photocurrent distribution profiles observed when an MJSC subcell is directly excited and when the LC effect is induced. To implement this model, first, we have developed a 2-D electrical circuit model.[19] Each unit is composed of three subcells representing the top, middle, and bottom cells as shown in Fig. 1. Here, the illuminated region is represented by units in white fill, whereas the perimeter region is represented by units in gray fill. The units are interconnected by a lumped series resistance R_s, which represents the current movement within the cell and the resistance between the metal contact and the cell. $J_{01,i}$ and $J_{02,i}$ represent the diffusion and the bulk nonradiative recombination diode coefficients with ideality factors of 1 and 2, respectively. $J_{0\mathrm{rad},i}$ is the radiative recombination diode coefficient of the i'th subcell with an ideality factor of 1. $J_{\mathrm{ph},i}$ is the generated photocurrent from external light sources in the i'th subcell. $R_{\mathrm{sh},i}$ is the shunt resistance of the i'th subcell.[20,21] $J_{\mathrm{LC},m\rightarrow \mathrm{b}}$ represents the generated LC current in the Ge bottom cell, which is dependent on the radiative recombination current of the GaAs middle cell.[9,12] The values of the parameters fitted with experimental data can be found in Table 4, Appendix A.3. As for the perimeter region, an ideality factor of 2 was assumed for the diode model per subcell representing the edge recombination.[14–18,22] In Fig. 1, this is labeled as $J_{02p,i}$. Then, the nonuniform illumination profile introduced by the LC effect is modeled using the equation of superellipse. This is further described in Sec. 2.3.

Assumptions were made to limit this study within the spatial LC effect from the GaAs middle cell to the Ge bottom cell. We assumed that the LC effect is negligible between the InGaP top cell

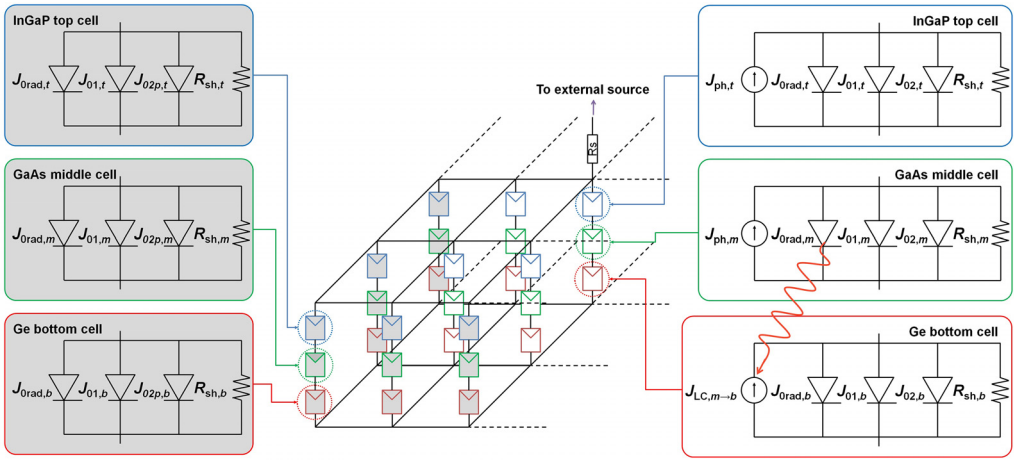

Fig. 1 A portion of the 2-D electrical circuit model for InGaP/GaAs/Ge 3JSC showing 9 cell units. The white-filled units represent those in the illuminated region while the gray-filled units represent those in the perimeter region.

and Ge bottom cell due to the optical thickness of the GaAs middle cell.[8,23] In addition, the photocurrent generation due to light unabsorbed by the upper subcells is much smaller compared with the LC current generation.[24] Thus, we assumed that all of the photocurrent generation in the Ge bottom cell by GaAs middle cell excitation is due to the LC effect. Also, the voltage distribution of the limiting Ge bottom cell is considered spatially uniform since the tunnel diode in between the GaAs and Ge subcells is heavily doped.[25] Hence, we assumed negligible tunneling resistance and lateral resistances. These assumptions then make the electrical circuit sufficient to expand in-plane, in 2-D. These simplifications also prevent having calculation artifacts and a long calculation time, which are encountered with increasing the number of nodes and components involved.

2.3 *Analytical Equations Used*

In the past literature, the equation of a superellipse has been assumed for modeling the Fraunhofer diffraction[26,27] and light scattering at textured surfaces of thin-film silicon solar cells.[28] This equation is given by

$$z_{\mathrm{opt}}(x,y) = \left(\frac{sxy}{k^2}\right)^2 - \left(\frac{x^2}{k^2} + \frac{y^2}{k^2}\right) + 1, \tag{1}$$

in Cartesian coordinates where s defines the sharpness of the superellipse corners. In this work, we introduce Eq. (1) to analytically model the nonuniform optical profile of the LC effect in MJSCs, in which x and y are defined as the in-plane distribution map positions and k is defined as half of the width of the cell sample. For square or rectangular-shaped solar cells, s is set to 1. This definition follows the criterion $k \geq \pm x, y$. Instead of implementing a Gaussian profile, which is typically assumed for modeling the illumination profile for distributed circuits considering spatial dependence of temperature effects in solar cells[29] and chromatic aberration, an optical effect in concentrator MJSC systems,[16,30,31] we opted to assume the superellipse profile. This is because the Gaussian profile contour is circular throughout the plane. On the other hand, the superellipse profile gradually changes from rectangular to a rounded rectangular shape toward the center of the cell, which better describes the observed LBIC maps.[13] Considering z_{opt}, the net electro-optical LC current $J_{\mathrm{LC,net}}(x,y)$ becomes

$$J_{\mathrm{LC,net}}(x,y) = [\beta_{\mathrm{LC}} z_{\mathrm{opt}}(x,y) + (1-\beta_{\mathrm{LC}})] J_{\mathrm{LC}}(x,y), \tag{2}$$

where β_{LC} is the fraction of nonuniformity describing the portion of the original local LC current, $J_{\mathrm{LC}}(x,y)$ that is laterally uniform.

To quantify the nonuniformity of the LC effect, the standard deviation of LC current map values σ_{LC} was calculated for every LBIC measurement. To calculate for the limiting cell conversion efficiency, the maximum power point voltage V_{mpp} from light $J-V$ characteristics was determined. From V_{mpp}, the nodal currents and voltages, $J_{mpp}(x,y)$ and $V_{mpp}(x,y)$, were extracted from the 2-D electrical circuit model. Then using the Q-2D simulation model, the nonuniform distribution of the LC effect was incorporated into $J_{mpp}(x,y)$ using Eq. (2). The cell conversion efficiency η_{TOTAL} was then calculated using

$$\eta_{TOTAL} = \frac{\iint J_{mpp}(x,y)V_{mpp}(x,y)\mathrm{d}x\,\mathrm{d}y}{P_{source}}, \tag{3}$$

where P_{source} is the incident light power per spot area and $\mathrm{d}x\,\mathrm{d}y$ is the differential cell area.

3 Results and Discussion

The lateral LBIC map for the GaAs middle cell acquired by direct 785-nm laser excitation is shown in Fig. 2(a). Here, we see that the distribution of photocurrent generation is uniform and an abrupt decrease is seen in the cell edges. Then, the lateral LBIC maps for the Ge bottom cell acquired by direct 1064-nm laser excitation and by LC effect (using 785-nm laser) are shown in Figs. 2(b) and 2(c), respectively. The photocurrent generation in the Ge bottom cell from direct excitation is uniform while from the LC effect, it shows increasing generation toward the center. To interpret Figs. 2(b) and 2(c), respectively, consider the illustrations shown in Figs. 2(d)–2(f). Figure 2(d) shows the direct excitation from the attenuated 1064-nm scanning laser, in which the Ge bottom cell was excited at its local points. Thus, the spatial distribution of photocurrent in this case was expectedly uniform. It is also noted that photocurrent is still high even near the cell edges, suggesting that the size of the perimeter where the edge recombination occurs in the Ge bottom cell is negligibly thin in this case. The observation is the same for direct GaAs middle excitation, as shown in Fig. 2(a). On the other hand, Figs. 2(e) and 2(f) show how the photons are emitted from some of the possible radiative emission spots in the GaAs middle cell toward the Ge bottom cell. Since the photocurrent generation due to the LC effect was observed to increase toward the cell center, assuming uniform voltage distribution across the Ge bottom cell, this suggests the following. One is that some of the photons emitted from the GaAs middle cell to the Ge bottom cell escape toward the edges via escape cone,[32] as shown in Fig. 2(e). Another is the internal reflection experienced by photons whose incident angles are larger than the escape cone, which may most likely arrive toward the center of the cell and be reabsorbed there, as shown in Fig. 2(f). These optical phenomena may thereby induce an in-plane nonuniformity,[33] which will be probed further in a future work.

Figures 2(g) and 2(h) show the lateral current maps without and with a nonuniform optical profile considered, respectively. In Fig. 2(g), the lateral current map is uniform because the 2-D electrical circuit calculations do not incorporate the nonuniform distribution profile of photons emitted from an adjacent higher bandgap subcell approaching the lower bandgap subcell of an MJSC. On the other hand, Fig. 2(h) shows a nonuniform lateral current map, after considering the nonuniform optical profile assumed. Here, the LC current increases toward the cell center as defined by Eq. (2). This assumption shows good agreement with the measured LC current distribution shown in Fig. 2(b). Thus, considering an optical profile, which is assumed as a superellipse distribution in our case, is necessary for modeling the nonuniform profile of the LC effect. This necessity also suggests that the spatial mismatch of the LC current generation in an MJSC subcell is mainly governed by its internal optics.

To determine how the LC current uniformity changes under different GaAs-to-Ge subcell LC efficiencies, using 785-nm excitation laser we acquired the LBIC maps under varying 660-nm LED intensity, thereby producing different LC efficiencies.[11] Figures 3(a)–3(d) show how increasing the GaAs-to-Ge subcell LC efficiency affects the nonuniformity of the LC current distribution map. These figures show that the LC current generated in the Ge bottom cell increases as the LC efficiency increases. However, with increasing LC efficiency, nonuniformity becomes more prominent in the LC current distribution. This is quantitatively confirmed by the standard deviation of LC current map values as summarized in Table 1. Here, a higher σ_{LC} value

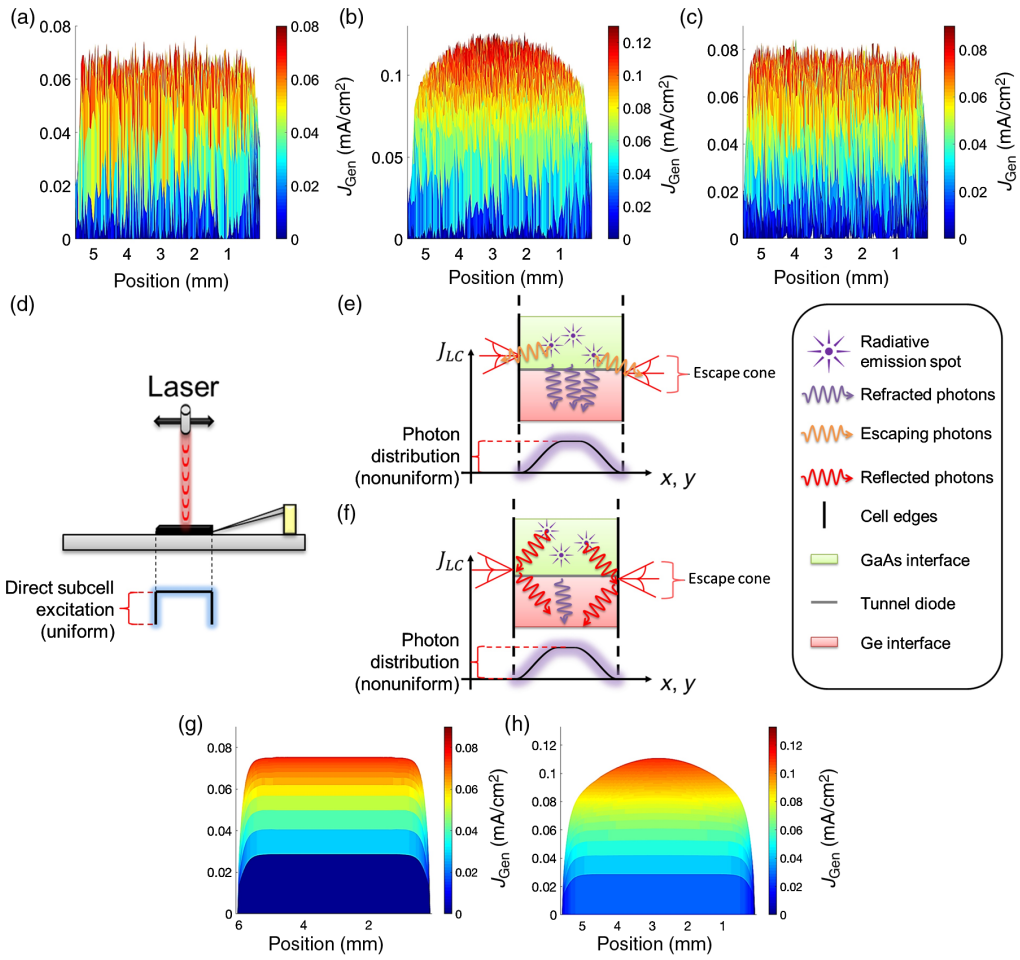

Fig. 2 Lateral LBIC maps of photocurrent generation (a) at GaAs middle cell by direct 785-nm laser excitation with ~90% attenuation filter and at Ge bottom cell (b) by LC effect using 785-nm laser and (c) by direct 1064-nm laser excitation with ~90% attenuation filter. (d) Illustration of 1064-nm laser excitation at a local point in Ge bottom cell. Some of the spontaneous emission spots in GaAs middle cell emitting photons toward Ge bottom cell, in which some photons are refracted (represented by violet waves), (e) other photons escape toward the cell edges (orange waves), (f) and other photons are internally reflected (red waves) during the LC effect, using 785-nm laser. Lateral view of the Q-2D current map extracts (g) without and (h) with nonuniformity of LC effect considered, respectively. Applied InGaP/GaAs/Ge 3JSC terminal voltage is 1.5 V and spatial resolution is 23.44×20.98 □/mm^2 for all current maps shown.

indicates less uniform current distribution. It is also noteworthy that the minimum and the maximum LC efficiencies derived from LBIC measurements fitting are 8.5% and 69%, respectively. 0% LC efficiency cannot be achieved experimentally because of measurement artifacts observed to become more severe at low photocurrent generation. Figures 3(e)–3(h) show the simulation results under various LC efficiencies. These results show good agreement with the measured LBIC maps, indicating the same inferences discussed for Figs. 2(b) and 2(h).

To probe the impact of a nonuniform LC effect to the limiting cell conversion efficiency, the Ge bottom cell conversion efficiency was calculated using Eq. (3). The Ge bottom cell conversion efficiency calculations are summarized in Table 1. Considering the nonuniform optical profile of the LC effect, calculations have shown that increasing LC efficiency yields increasing Ge bottom cell efficiency as well. On the other hand, comparing the Ge bottom cell conversion efficiency calculations with ($\beta_{LC} \neq 0$, assimilated from LBIC measurements) and without ($\beta_{LC} = 0$) the optical nonuniformity considered, about 1.35% absolute conversion efficiency reduction is introduced at the highest LC efficiency, which is relatively 16.83% of the Ge bottom cell conversion efficiency if the LC effect is uniformly distributed. With this amount of subcell

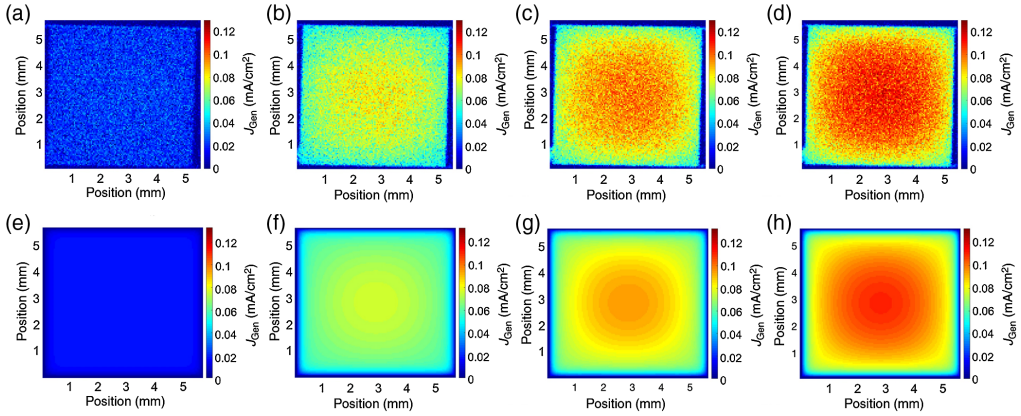

Fig. 3 Color map representations of LC current distribution at Ge bottom cell whose LC efficiencies are (a) and (e) 8.5%, (b) and (f) 18%, (c) and (g) 41%, and (d) and (h) 69%. Here, (a)–(d) were experimentally acquired from LBIC measurements employing 785-nm excitation laser under varying 660-nm LED intensities whereas (e)–(h) were acquired from Q-2D simulation. Applied InGaP/GaAs/Ge 3JSC terminal voltage is 1.5 V for all current maps shown.

Table 1 Summary of standard deviation of LC current map values obtained from LBIC map and calculated conversion efficiencies from the Q-2D power distribution maps with increasing GaAs-to-Ge subcell LC efficiencies where Ge bottom cell is limiting. Values shown were rounded up to the nearest hundredths.

			η_{TOTAL}[d] (%)			
$P_{LED,660\ nm}$[a] (mW/cm^2)	$\alpha_{LC,m\to b}$[b] (%)	$\sigma_{J_{LC}}$[c] (μA/cm^2)	Nonuniform LC (assimilated, $\beta_{LC} \neq 0$)	Uniform LC ($\beta_{LC} = 0$)	$\Delta\eta_{TOTAL}$[e] (%)	$\Delta\eta_{reduction}$[f] (%)
35.00	8.50	9.50	0.00	0.00	0.00	0.00
180.00	13.00	21.60	1.34	1.53	0.20	12.77
200.00	18.00	23.40	2.57	2.95	0.38	12.76
225.00	27.00	26.00	3.80	4.40	0.60	13.57
240.00	35.00	27.30	4.58	5.37	0.78	14.62
250.00	41.00	28.40	4.90	5.82	0.92	15.73
270.00	56.00	29.80	6.02	7.15	1.13	15.77
293.46	69.00	33.50	6.67	8.01	1.35	16.83

[a] $P_{LED,660\ nm}$ is the 660-nm continuous LED light intensity.
[b] $\alpha_{LC,m\to b}$ is the LC efficiency from GaAs to Ge subcell.
[c] $\sigma_{J_{LC}}$ is the standard deviation of LC current map values.
[d] η_{TOTAL} is the Ge bottom cell conversion efficiency.
[e] $\Delta\eta_{TOTAL}$ is the absolute conversion efficiency difference between having uniform ($\beta_{LC} = 0$) and nonuniform ($\beta_{LC} \neq 0$) LC current at Ge bottom cell.
[f] $\eta_{reduction}$ is the relative Ge bottom cell conversion efficiency reduction due to nonuniform LC effect.

conversion efficiency reduction, spatial current matching becomes an important concept to further improve the MJSC conversion efficiency when benefitting from the LC effect.

4 Conclusion

Nonuniform LC current generation was observed in the Ge bottom cell of an InGaP/GaAs/Ge 3JSC when it was made current limiting. Good agreement of experiment and simulation results

suggests that the nonuniform LC effect in MJSCs is optically induced. This is possibly caused by photons emitted from a higher bandgap subcell to a lower bandgap subcell escaping toward the cell edges and by internally reflected photons getting better absorbed toward the center of the cell. At maximum GaAs-to-Ge subcell LC efficiency, although the conversion efficiency of the Ge bottom cell that may be achieved was calculated at 8.01% for a cell area of 0.31 cm^2, the absolute conversion efficiency reduction introduced by a nonuniform LC effect was calculated at 1.35%. From our results, it can then be inferred that the limiting Ge bottom cell conversion efficiency can be further improved by making the LC current generation spatially uniform. This can be done by finding ways to improve current generation toward the cell perimeter in order to compensate for the loss due to the nonuniform current generation of a strong LC effect especially for MJSC structures intentionally designed for concentrator photovoltaic systems.

Appendix

A.1 Comparison of Increased Perimeter Area and Optically Induced Nonuniformity of Luminescence Coupling Effect

Figure 4 shows the simulated LC current distribution maps with varying spatial LC current distribution profiles and varying perimeter areas. Figures 4(a) and 4(b) show a uniform LC current profile, but have thin and thick perimeter areas, respectively. Figure 4(c) shows the same as the one shown in Fig. 3(h) and was included in this set of figures for convenience. Comparing Figs. 4(a) and 4(b), it can be seen that the difference in current distributions between the bulk and the perimeter regions is abrupt. On the other hand, comparing Figs. 4(a) and 4(c), the current distribution difference between the bulk and the perimeter regions is gradual. Thus, the approach for modeling edge recombination effects and the optically nonuniform LC effect is not the same as they yield different results.

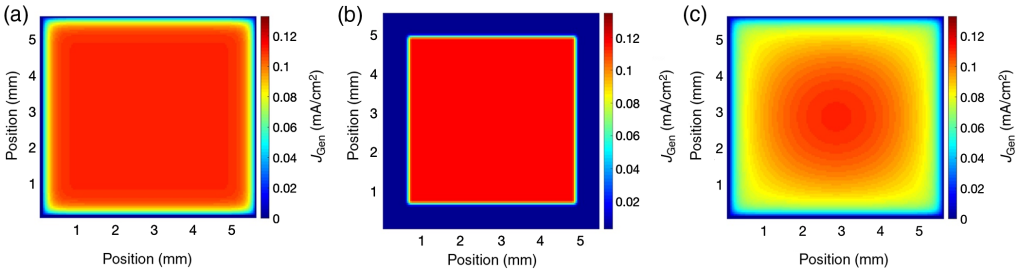

Fig. 4 Simulated Ge bottom cell LC current distribution profiles with (a) uniform profile, thin perimeter area, (b) uniform profile, perimeter area thicker than that in (a), and (c) nonuniform profile, thin perimeter area.

Table 2 Summary of continuous LED sources specifications used for LBIC measurements.

LED wavelength (nm)	Maximum power density (mW/cm^2)
430[a,b]	47.50
660[b]	293.46
970[a]	30.84
1550[a]	3.50

[a]LEDs used to current-limit the GaAs middle cell.
[b]LEDs used to current-limit the Ge bottom cell.

Table 3 Summary of pulsating laser sources specifications used for LBIC measurements.

Laser wavelength (nm)	Spot size (μm)	Measured power, no filter (μW)	Power density, no filter (mW/cm^2)	Measured power, with filter[b] (μW)	Power density, with filter[b] (mW/cm^2)
785	50	51.00	2597.41[a]	5.70	290.30
1064	100	53.40	679.91	5.85	74.48

[a]Power density, P_{source}, used for calculating the limiting cell conversion efficiencies listed in Table 1.
[b]~90% attenuation filter.

Table 4 Summary of parameter values used for each subcell of the InGaP/GaAs/Ge 3JSC fitted into the 2-D electrical circuit SPICE model with experiment data. Here, dA is the differential cell area.

Parameters fitted	InGaP top cell	GaAs middle cell	Ge bottom cell
Diffusion diode coefficient $J_{01,i}$ (mA/dA)	1.00×10^{-30}	1.00×10^{-26}	9.00×10^{-12}
Nonradiative recombination diode coefficient $J_{02,i}$ (mA/dA)[a]	1.20×10^{-18}	1.67×10^{-13}	1.00×10^{-9}
Radiative recombination diode coefficient $J_{0Rad,i}$ (mA/dA)	2.16×10^{-29}	1.64×10^{-21}	6.75×10^{-11}
Shunt resistance $R_{SH,i}$ (Ω/dA)	6.50×10^{14}	1.60×10^{9}	2.50×10^{7}
Lumped series resistance R_S (Ω)		1.20	

[a]The same parameters used for $J_{02p,i}$.

A.2 Specifications of Light Sources Employed

Tables 2 and 3 summarize the specifications of the continuous LED and pulsating laser sources employed in the LBIC measurement setups described in Sec. 2.1, respectively.

A.3 Electrical Circuit Model Parameters Fitted

Table 4 shows the list of parameters used upon assimilating the measurement data into the 2-D electrical circuit model.

Acknowledgments

This work is performed under Research and Development of ultrahigh efficiency and low-cost III-V compound semiconductor solar cell modules supported by the National Research and Development Agency, New Energy and Industrial Technology Development Organization (NEDO), and Ministry of Economy, Trade, and Industry (METI), Japan. The authors declare no competing financial interests or other potential conflict of interests.

References

1. R. R. King et al., "Advances in high-efficiency III-V multijunction solar cells," *Adv. OptoElectron.* **2007**, 29523 (2007).
2. F. Dimroth and S. Kurtz, "High-efficiency multijunction solar cells," *MRS Bull.* **32**, 230–235 (2007).
3. M. A. Green et al., "Solar cell efficiency tables (version 47)," *Prog. Photovoltaics Res. Appl.* **24**, 3–11 (2016).

4. C. Baur et al., "Effects of optical coupling in III-V multilayer systems," *Appl. Phys. Lett.* **90**(19), 192109 (2007).
5. K. H. Lee et al., "Demonstration of photon coupling in dual multiple-quantum-well solar cells," *IEEE J. Photovoltaics* **2**(1), 68–74 (2012).
6. D. Derkacs, D. T. Bilir, and V. A. Sabnis, "Luminescent coupling in GaAs/GaInNAsSb multijunction solar cells," *IEEE J. Photovoltaics* **3**(1), 520–527 (2013).
7. D. J. Friedman, J. F. Geisz, and M. A. Steiner, "Analysis of multijunction solar cell current-voltage characteristics in the presence of luminescent coupling," *IEEE J. Photovoltaics* **3**(4), 1429–1436 (2013).
8. M. A. Steiner et al., "Measuring IV curves and subcell photocurrents in the presence of luminescent coupling," *IEEE J. Photovoltaics* **3**(2), 879–887 (2013).
9. D. J. Friedman, J. F. Geisz, and M. A. Steiner, "Effect of luminescent coupling on the optimal design of multijunction solar cells," *IEEE J. Photovoltaics* **4**(3), 986–990 (2014).
10. M. Z. Shvarts et al., "Method for direct measurements of luminescent coupling efficiency in concentrator MJ SCs," in *AIP Conf. Proc.*, Vol. 1556, No. 1, p. 147 (2013).
11. T. Sogabe et al., "Experimental characterization and self-consistent modeling of luminescence coupling effect in III-V multijunction solar cells," *Appl. Phys. Lett.* **103**(26), 263907 (2013).
12. C. R. Allen et al., "Simple method for determining luminescence coupling in multi-junction solar cells," in *37th IEEE Photovoltaic Specialists Conf. (PVSC '11)*, p. 452 (2011).
13. B. M. Yu Jeco et al., "Laser beam induced current (LBIC) mapping of InGaP/GaAs/Ge triple junction solar cells with luminescence coupling," in *IEEE 43rd Photovoltaic Specialists Conf. (PVSC '16)*, pp. 1229–1234 (2016).
14. K. R. McIntosh and C. B. Honsberg, "The influence of edge recombination on a solar cell's IV curve," in *Proc. 16th PV Solar Energy Conf. and Exhibition*, pp. 1651–1654 (2000).
15. M. Hermle et al., "Analysis of edge recombination for high-efficiency solar cells at low illumination densities," in *Proc. IEEE 3rd World Conf. on Photovoltaic Energy Conversion*, Vol. 2, p. 1009 (2003).
16. I. García et al., "Analysis of chromatic aberration effects in triple-junction solar cells using advanced distributed models," *IEEE J. Photovoltaics* **1**(2), 219–224 (2011).
17. P. Espinet-González et al., "Analysis of the behavior of multijunction solar cells under high irradiance Gaussian light profiles showing chromatic aberration with emphasis on tunnel junction performance," *Prog. Photovoltaics Res. Appl.* **23**(6), 743–753 (2015).
18. B. Galiana et al., "A 3-D model for concentrator solar cells based on distributed circuit units," *IEEE Trans. Electron Devices* **52**(12), 2552–2558 (2005).
19. K. Nishioka et al., "Analysis of triple-junction solar cell under concentration by SPICE," in *Proc. IEEE 3rd World Conf. on Photovoltaic Energy Conversion*, Vol. 1, p. 869 (2003).
20. J. Nelson, *The Physics of Solar Cells*, Imperial College, London (2003).
21. M. A. Green, *Solar Cells: Operating Principles, Technology and System Applications*, The University of New South Wales, New South Wales (1998).
22. P. Espinet-González et al., "Analysis of perimeter recombination in the subcells of GaInP/GaAs/Ge triple-junction solar cells," *Prog. Photovoltaics Res. Appl.* **23**(7), 874–882 (2015).
23. H. C. Casey, Jr., D. D. Sell, and K. W. Wecht, "Concentration dependence of the absorption coefficient for n- and p- type GaAs between 1.3 and 1.6 eV," *J. Appl. Phys.* **46**(1), 250–257 (1975).
24. J. J. Li et al., "Combined effects of shunt and luminescence coupling on external quantum efficiency measurements of multijunction solar cells," *IEEE J. Photovoltaics* **1**(2), 225–230 (2011).
25. M. Yamaguchi et al., "Multi-junction III-V solar cells: current status and future potential," *Sol. Energy* **79**(1), 78–85 (2005).
26. M. F. Guasti and M. D. L. C. Heredia, "Diffraction pattern of a circle/square aperture," *J. Mod. Opt.* **40**(6), 1073–1080 (1993).
27. M. F. Guasti et al., "LCD pixel shape and far-field diffraction patterns," *Optik* **116**(6), 265–269 (2005).
28. M. Zeman et al., "Advanced light management approaches for thin-film silicon solar cells," *Energy Procedia* **15**, 189–199 (2012).

29. E. Franklin and J. Coventry, "Effects of highly non-uniform illumination distribution on electrical performance of solar cells," in *ANZSES Solar Conf.* (2002).
30. M. Victoria et al., "Characterization of the spatial distribution of irradiance and spectrum in concentrating photovoltaic systems and their effect on multi-junction solar cells," *Prog. Photovoltaics Res. Appl.* **21**(3), 308–318 (2013).
31. R. Herrero et al., "Concentration photovoltaic optical system irradiance distribution measurements and its effect on multi-junction solar cells," *Prog. Photovoltaics Res. Appl.* **20**(4), 423–430 (2012).
32. E. F. Schubert, *Light-Emitting Diodes*, Cambridge University Press, New York (2003).
33. B. E. Saleh and M. C. Teich, *Fundamentals of Photonics*, John Wiley & Sons, Inc., New Jersey (2007).

Bernice Mae F. Yu Jeco received her BS degree in electronics and communication engineering from the University of Santo Tomas in 2011 and her master's of engineering degree in electrical engineering and information systems from the University of Tokyo (UT) in 2017. She is a PhD candidate in the Department of Advanced Interdisciplinary Studies, UT. Her current research interests include high-efficiency tandem solar cells and quantum dot solar cells.

Nazmul Ahsan received his BE in electrical and electronic information engineering from Toyohashi University of Technology, Japan, in 1997, his MS and PhD degrees in electronic engineering from The University of Tokyo (UTokyo), Japan, in 1999 and 2002, respectively. He then held a Japan Science and Technology Agency (JST) research fellowship at UT, and worked on light and electric field control of ferromagnetism using III-V heterostructures. He is currently a project associate professor at the Research Center for Advanced Science and Technology (RCAST), UTokyo. His research interests include ultra high-efficiency photovoltaic devices, spintronic devices, and molecular beam epitaxy of compound semiconductors. His articles have more than 1000 citations (Google Scholar).

Biographies for the other authors are not available.